Interfacial coupling between ferromagnets and random and dilute antiferromagnets

Kineshma Munbodh, Miyeon Cheon, David Lederman, M. R. Fitzsimmons, and Neil R. Dilley

Phys. Rev. B **84**, 214434 — Published 22 December 2011

DOI: 10.1103/PhysRevB.84.214434

Interface coupling between ferromagnets and random and dilute antiferromagnets

Kineshma Munbodh,* Miyeon Cheon, and David Lederman
Department of Physics, West Virginia University, Morgantown, WV 26506-6315, USA

M. R. Fitzsimmons
Los Alamos National Laboratory, Los Alamos, NM 87545, USA.

Neil R. Dilley
Quantum Design, Inc., San Diego, CA 92121, USA
(Dated: December 6, 2011)

Depth profiles for pinned and unpinned magnetizations were determined across the interface between a ferromagnet (F) and random and dilute antiferromagnets (RAF and DAF) exemplified by $Fe_{0.45}Ni_{0.55}F_2$/Co and $Fe_{0.34}Zn_{0.66}F_2$/Co bilayers, respectively, using polarized neutron reflectivity (PNR). PNR measurements were complemented by magnetometry using applied fields as large as 160 kOe to assure saturation of the entire sample, including magnetic moments that are normally pinned at lower fields. The locations of pinned and unpinned magnetization in the ferro- and antiferromagnets were identified. The origin of exchange bias in the RAF system is noticeably different than that of the DAF system. In the RAF system, a domain wall is formed at the RAF/F interface when the ferromagnet's magnetization is reversed. In the DAF system, some domains within the bulk of the DAF are reversed upon reversal of the ferromagnet while others remain pinned. In this case, the interface magnetization is entirely reversed.

PACS numbers: 75.70.-i, 75.70.Cn, 75.30.Gw, 75.50.Ee

I. INTRODUCTION

Exchange bias (EB) has been extensively investigated since its discovery[1] as a means to pin magnetization in spin-valve electronic devices.[2,3] Its characteristic feature is the shift of the magnetic hysteresis loop of a ferromagnet (F) along the field axis by an amount H_E due to a coupling of the F to an antiferromagnet (AF) after cooling the sample from above the AF Néel temperature (T_N) in an applied cooling field H_{CF}.

Most EB theories rely on uncompensated spins in the AF for an AF/F coupling mechanism.[4] In order to test the importance of uncompensated spins, EB measurements have been carried out on dilute AF/F $Co_xMg_{1-x}O$/Co bilayers where an enhancement of a factor of two or greater of the EB was observed for dilutions of $x \approx 0.80$ because of uncompensated spins that form at the AF domain boundaries (domain state model).[5–7] $Fe_xZn_{1-x}F_2$ is also a dilute antiferromagnet (DAF) which behaves as a random field Ising model system.[8] In twinned $Fe_{0.83}Zn_{0.17}F_2/FeF_2$/Co bilayers, a 65% increase of H_E has been observed with respect to pure FeF_2/Co bilayers,[9] although in single-crystalline (untwinned) $Fe_xZn_{1-x}F_2$/Co bilayers there is no significant enhancement of the EB, presumably due to less disorder and a lack of percolation of non-magnetic impurities at higher Fe concentrations.[10]

Recently, uncompensated Fe spins at the AF/F FeF_2/Co interface were observed using x-ray magnetic circular dichroism.[11,12] Additional evidence for the existence of uncompensated spins within the bulk FeF_2 antiferromagnetic layer has been obtained using polarized neutrons and soft x-ray magnetic scattering.[11,13] Among the uncompensated spins, some are pinned, which results in a shift of the hysteresis loop along the magnetization (vertical) axis, in addition to the shift along the magnetic field (horizontal) axis normally associated with H_E. The shift due to the pinned spins can be defined as $\Delta M_S = (M_S^+ + M_S^-)/2$, where M_S^+ and M_S^- are the saturation magnetization values at positive and negative fields, respectively. In pure FeF_2/Co bilayers, ΔM_S is small and difficult to detect via conventional magnetometry, and its magnitude depends strongly on H_{CF} and microstructure of the AF layer.[14] On the other hand, a relatively large pinned uncompensated spin has been observed via conventional magnetometry in $Fe_xZn_{1-x}F_2$/Co bilayers.[10]

Another system that also has a significant ΔM_S is the $Fe_xNi_{1-x}F_2$/Co bilayer,[15] where $Fe_xNi_{1-x}F_2$ is an AF with a random anisotropy. FeF_2 and NiF_2 are antiferromagnets that have the same rutile crystal structure,[16] but while FeF_2 has a strong uniaxial anisotropy along the [001] c-axis direction,[17,18] NiF_2 has an in-plane (001) anisotropy[19,20] with a Dzialoshinskii-Moriya interaction that makes this compound a weak ferromagnet.[21] Because the effective magnetic anisotropy fields in these two compounds are perpendicular to each other, the $Fe_xNi_{1-x}F_2$ alloy is an ideal tunable system to study the role of AF magnetic anisotropy in EB.[15] Here we refer to this system as a random antiferromagnet/ferromagnet bilayer (RAF/F). In this system, a positive EB has also been observed, which means that a positive cooling field results in a positive H_E.[22–25] A proposed mechanism for positive EB requires that an AF/FM system have both antiferromagnetic coupling at the interface and an uncompensated magnetization in the AF. As the sample is field-cooled through T_N, the uncompensated magnetization could line up either parallel or antiparallel to the FM, depending on the strength of the cooling field. A large cooling field results in a positive EB because the system is frozen in a high interface energy configuration.[23]

Here we describe an investigation of the relationship between EB and pinned magnetization using magnetometry and polarized neutron reflectivity (PNR) for $Fe_{0.45}Ni_{0.55}F_2$/Co and $Fe_{0.34}Zn_{0.66}F_2/FeF_2$/Co multilayers, that is, model RAF/F and DAF/F systems. These samples have a significant pinned magnetization that can be easily measured via standard magnetometry techniques. These samples have different mechanisms responsible for the EB. In the RAF/F sample, PNR showed that the pinned magnetization at the RAF/F interface tended to be antiparallel to the FM magnetization, which is consistent with antiferromagnetic coupling. Moreover, a domain wall was created at the interface in the exchange-biased state. On the other hand, the DAF/F system's interface magnetization was completely unpinned. Within the bulk of the DAF, some domains were also unpinned, but their net magnetizations were effectively coupled antiferromagnetically to the ferromagnet, while some pinned domains remained. These results are discussed in view of prior experimental and theoretical results.

II. EXPERIMENTAL PROCEDURES

A. Sample Growth

The two samples used in this study were grown on MgF_2 (110) single crystal substrates via molecular beam epitaxy as described elsewhere.[10,26] One sample consisted of a RAF/F $Fe_{0.45}Ni_{0.55}F_2$ (370 Å)/Co (80 Å) bilayer while the other consisted of a DAF/F $Fe_{0.34}Zn_{0.66}F_2$ (230 Å)/FeF_2 (10 Å)/Co (150 Å) multilayer. The pure FeF_2 layer between the $Fe_{0.34}Zn_{0.66}F_2$ and Co layers was inserted to produce a larger AF/FM coupling.[10] In both samples the AF layers were single-crystalline and oriented along the [110] direction while the Co layer was polycrystalline. Both samples

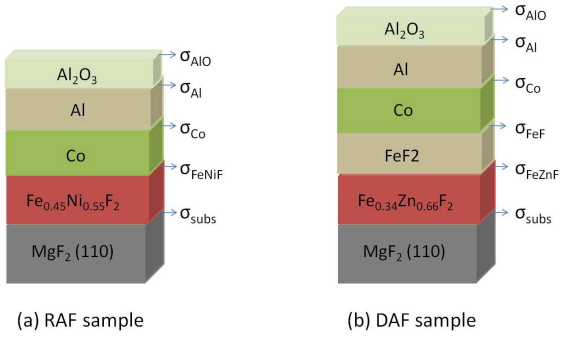

FIG. 1. (Color Online) Sketch of (a) RAF $Fe_{0.45}Ni_{0.55}F_2$/Co and (b) DAF $Fe_{0.34}Zn_{0.66}F_2$/FeF_2/Co samples used in XRR model. The location of the interface roughness σ and the layers used in the fitting model are indicated.

were capped by Al to prevent oxidation. The Fe concentrations in the DAF and RAF layers were determined from x-ray diffraction measurements of the in-plane [001] lattice parameter.[9]

B. X-ray Reflectivity

The non-magnetic structure of the samples was determined by analyzing the x-ray reflectivity (XRR) using GenX,[27] a software package which uses the Parratt recursion formalism[28] for simulation and a genetic algorithm for parameter optimization. The model used to fit XRR data is illustrated in Figs. 1(a) and 1(b) for the $Fe_{0.45}Ni_{0.55}F_2$/Co and $Fe_{0.34}Zn_{0.66}F_2$/FeF_2/Co samples, respectively. From this model it was possible to obtain the x-ray charge scattering length density profile $\rho_{xr}(z)$, where z is defined as the distance from the substrate/AF interface.[29] The derivative $d\rho_{xr}/dz$ was used to determine each layer's thickness t and the roughness at each interfaces σ as described in the Appendix of Ref. 29.

C. Magnetometry

The magnetic properties of the RAF $Fe_{0.45}Ni_{0.55}F_2$ sample were measured via a Quantum Design Physical Measurement System (PPMS) equipped with a vibrating sample magnetometer in the range of $H = \pm 160$ kOe and $H = \pm 110$ kOe at $T = 30$ K after cooling from room temperature in a field of $H_{CF} = 2$ kOe along the in-plane [001] direction, which is the magnetic easy axis of FeF_2. To take into account the remanent field due to trapped flux in the superconducting magnet coils, it was necessary to measure a standard paramagnetic Dy_2O_3 pellet which exhibits no hysteresis.[30] This was done at $T = 300$ K in the field range of $H = \pm 16$ T with the same field step size and procedure used in measuring the RAF sample. The difference in field between the same magnetization values when ramping up and down in field was fitted to a Voigt line shape and the result was used to adjust the actual value of the magnetic field. This correction was probably not as accurate for the $H = \pm 11$ T RAF magnetization data discussed below because the field range was different, but in that case we compare with PNR measurements performed at higher fields ($|H| \geq 1$ T) where the correction is small.

The magnetic properties of the DAF $Fe_{0.34}Zn_{0.66}F_2$ sample were measured using a Quantum Design Magnetic Properties Measurement System (MPMS) SQUID magnetometer with H applied along the DAF [001] easy axis direction. The samples were cooled from $T = 95$ K$> T_N = 78.4$ K of FeF_2 to $T = 5$ K with values of H_{CF} ranging from 100 Oe to 7500 Oe. Hysteresis loops in the range of $T = 5$ K to $T = 300$ K were measured for -10 kOe $\leq H \leq +10$ kOe.

D. Polarized Neutron Reflectivity

PNR was measured at Los Alamos National Laboratory using the Asterix spectrometer. The data were corrected for the imperfect polarization of the neutron beam and wavelength variation in the neutron spectrum after removing the instrumental background corresponding to a reflectivity of order 10^{-7}.[13] Previous work on $Fe_xNi_{1-x}F_2$/Co bilayers[15,26]

has shown that a large amount uncompensated magnetization is pinned and its sign is correlated with that of the EB. It has also been shown that the pinned magnetization could be unpinned by sufficiently high fields.[15,26] The aim of the present experiments was to determine the location of the pinned magnetization.

The RAF/F $Fe_{0.45}Ni_{0.55}F_2$/Co sample was measured at $T = 30$ K in a superconducting magnet. Scattering cross-sections corresponding to the non-spin-flip reflectivity profiles for spin-up (R^{++}) and spin-down (R^{--}) neutron beam polarizations were measured at $H = +110, +10, -10, -110,$ and $+10$ kOe, in that order. By reversing as much of the RAF/F sample's magnetization as possible, in the ferromagnet, interface, and antiferromagnet layers, we were able to probe both the pinning mechanism as well as the complete reversal process at large fields.

R^{++} and R^{--} reflectivity profiles were measured on the DAF/F $Fe_{0.34}Zn_{0.66}F_2$/Co sample after cooling to $T = 5$ K with $H_{CF} = 2$ kOe applied along the DAF [001] direction in a closed-cycle refrigerator cryostat. The fields applied to the sample during the neutron measurments were ± 6.5 kOe. For these experiments H was provided by a conventional electromagnet. For the DAF/F system, we have found that it was impossible to reverse magnetization generated in the DAF during the cool-down procedure using fields of up to 70 kOe, unless the temperature was very close to the DAF transition temperature (data not shown).

PNR data were fitted using the GenX software package[27] with a scattering model consisting of three different magnetic layers corresponding to the FM, interface region, and AF, as described in Ref. 13. By fitting the R^{++} and R^{--} data simultaneously, the depth profiles of the nuclear (ρ_n) and magnetic (ρ_m) scattering length density profiles were extracted from the spin-dependent neutron-scattering length density $\rho = \rho_n \pm \rho_m$, where $\rho_m = M \times 2.853 \times 10^{-9}$ Å^{-2}cm^3/emu, and M is the magnetization of the sample in emu/cm^3. The actual thickness of the layers and roughness at each interface were obtained from $d\rho_n/dz$ and the uncertainties of the fitted parameters were calculated using a Monte Carlo data analysis procedure.[29,31]

For the RAF/F $Fe_{0.45}Ni_{0.55}F_2$/ Co sample, all the structural and magnetic parameters were fitted for the R^{++} and R^{--} data obtained at $H = +110$ kOe. For data obtained at other fields, only the magnetizations of the RAF, interface, and F layers were fitting parameters. The structural parameters were constrained to be the same as those obtained for the $H = +110$ kOe fits.

For the DAF/F $Fe_{0.34}Zn_{0.66}F_2$/Co sample, all structural parameters and magnetizations of the DAF, interface, and F layers were fitted for the R^{++} and R^{--} data measured at $H = -6.5$ kOe. For data measured at $H = +6.5$ kOe, the structural parameters were constrained to be the same as those obtained obtained at $H = -6.5$ kOe while the magnetizations of the AF, interface, and FM layers were used as fitting parameters.

III. RESULTS AND DISCUSSION

A. RAF $Fe_{0.45}Ni_{0.55}F_2$/Co Sample

Figure 2(a) shows the XRR data and their corresponding fit, while Fig. 2(b) shows $\rho_{xr}(z)$ and $d\rho_{xr}/dz$ obtained from the fit. The best fitting parameters and the associated uncertainties are listed in Table I. Results from fits to the PNR data are also listed. Note that no interface layer is explicitly listed for the XRR data. For the PNR data analysis, this layer had to be added explicitly in order to obtain the magnetization profile.

The hysteresis loops of the RAF/F $Fe_{0.45}Ni_{0.55}F_2$/Co sample are shown Fig. 3. When the sample was cooled in a field $H_{CF} \sim 100$ Oe, it had a negative EB of $H_E = -175$ Oe. As H_{CF} was increased, the EB gradually increased and eventually became postive. This behavior suggests that the exchange coupling between F and DAF is antiferromagnetic.[11,14,23] This is due to the details of the interface structure of this particular sample since the amount of interface disorder is known to affect the sign of the exchange bias in pure FeF_2/Fe bilayers,[23] and is probably not a result of the presence of Ni in the DAF layer.

The measurements for $H_{CF} = 2000$ Oe show a double hysteresis loop, with approximately 1/4 of the magnetization having a negative EB of $H_E = -750$ Oe, and the remaining magnetization having a positive EB of $H_E = 750$ Oe. The entire hysteresis loop had a positive pinned magnetization $\Delta M_S/M_S = 0.04$. Interestingly, there was no difference in the magnetization loops measured in the ranges of $H = \pm 10$ kOe and $H = \pm 70$ kOe, both having the same amount of pinned magnetization, unlike other $Fe_xNi_{1-x}F_2$/Co samples where a step in the magnetization, indicative of pinned magnetization reversal in the RAF, was observed at fields lower than 70 kOe.[15,26] Therefore, higher field scans were performed between $H = \pm 160$ kOe (for the magnetization measurements) and $H = \pm 110$ kOe (for the PNR measurements) to reverse the RAF pinned magnetization as much as possible.

For the hysteresis curves measured in the range of $H = \pm 160$ kOe, shown in Fig. 4, the most distinctive features are: (1) the hysteresis present at high fields, (2) the absence of ΔM_S ($0.007 \pm 0.02 \times 10^{-4}$) emu , in contrast to data taken between ± 10 kOe or ± 70 kOe, (3) the absence of EB, and (4) the reversed magnetization hysteresis shown in Fig. 4(b). The hysteresis at high fields can be interpreted as a reversal of the pinned magnetization and therefore $\Delta M_S = 0$. Because the pinned magnetization is reversed by the applied field, there was no EB as has been shown

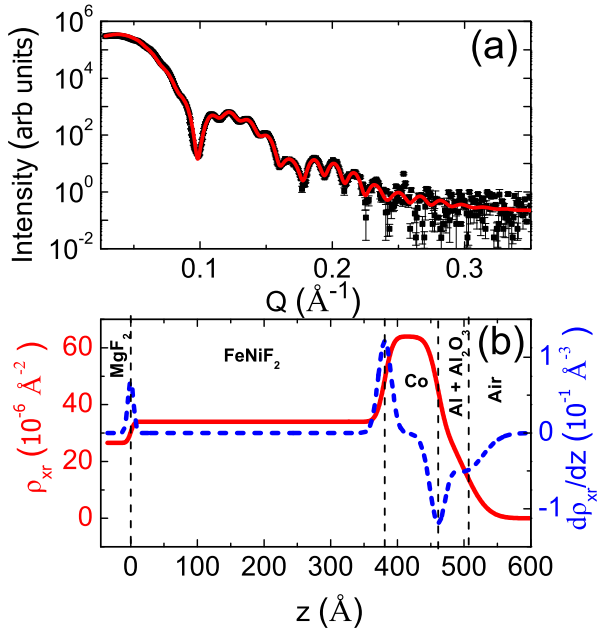

FIG. 2. (Color Online)(a) X-ray reflectivity measurements (black dots) and fit (red curve) of RAF $Fe_{0.45}Ni_{0.55}F_2$/Co sample and (b) the x-ray charge scattering length density profile (red curve) and its derivative (blue dashed curve) obtained from the fit. The vertical dotted lines indicate the positions of the interfaces, with the substrate-film interface set at $z = 0$.

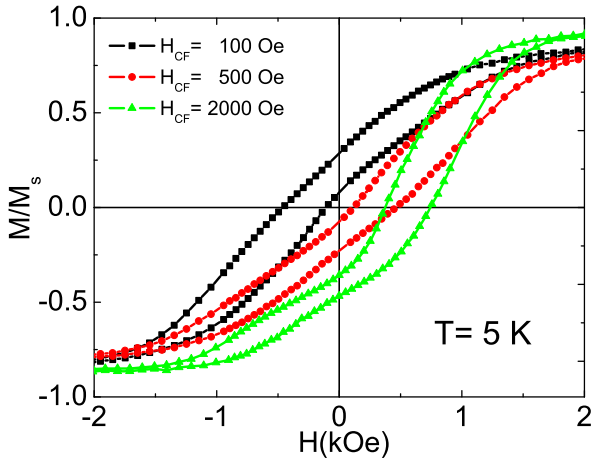

FIG. 3. (Color Online) Hysteresis loop of the RAF/F $Fe_{0.45}Ni_{0.55}F_2$/Co sample at $T = 5$ K after cooling at different fields. The hysteresis loop were measured in the range of $H = \pm 10$ kOe applied along the direction of the c-axis of the $Fe_{0.45}Ni_{0.55}F_2$ layer.

elsewhere.[15,26] The reversed magnetization loop in Fig. 4(b) means that $M \approx 0$ at a positive field when the field was decreased and $M > 0$ at a negative field when the field was increased. This is consistent with antiferromagnetic exchange coupling at the RAF/F interface, which can be responsible for positive EB.[23] At very large fields, the (normally) pinned layer magnetization at the interface is reversed. As the field was lowered, the process led to an effective coercivity $H_{C,\text{eff}} \approx -H_C + H_E$, where H_C is the normal coercive field. For the positive EB of the loop in Fig. 3, we have $H_E = 750$ Oe and $H_C = 250$ Oe. Hence, we could expect $H_{C,\text{eff}} = 500$ Oe, which is approximately what is observed for the upper part of the loop in Fig. 4(b). The reversed hysteresis loop is therefore a direct consequence of the antiferromagnetic coupling at the RAF/F interface. This has not been observed before in samples with positive exchange bias because normally the pinned magnetization in the AF cannot be reversed at low temperatures. Here, the sample was cooled in order to establish the positive exchange bias, and then the DAF magnetization was reversed at low temperature by the large applied field at the extremes of the hysteresis loop.

TABLE I. Structural fitting parameters determined from PNR and XRR data for the RAF/F $Fe_{0.45}Ni_{0.55}F_2$/Co sample. Interface roughness σ and layer thickness t parameters are in Å while the nuclear and x-ray charge scattering lengths, ρ_n and ρ_{xr}, are in 10^{-6} Å^{-2}. PNR measurements were performed at $H = 110$ kOe. Parameters without uncertainties were kept constant during the fitting procedure.

Layer	Parameter	PNR	XRR
Al_2O_3	ρ_n, ρ_{xr}	1.1	17.5
	σ	10 ± 4	7 ± 3
	t	16 ± 9	14 ± 4
Al	ρ_n, ρ_{xr}	1.6	29.2
	σ	17 ± 6	18 ± 3
	t	26 ± 7	27 ± 4
Co	ρ_n, ρ_{xr}	2.02	63.9
	σ	14 ± 7	11 ± 3
	t	81 ± 7	80 ± 4
Interface	ρ_n	2.79 ± 0.06	
	σ	5 ± 2	
	t	36 ± 8	
$Fe_{0.45}Ni_{0.55}F_2$	ρ_n, ρ_{xr}	5.64 ± 0.04	34 ± 1
	σ	15 ± 5	12 ± 3
	t	342 ± 9	381 ± 3
MgF_2	ρ_n, ρ_{xr}	5.1	26.5
(Substrate)	σ	5 ± 1	4.2 ± 0.8

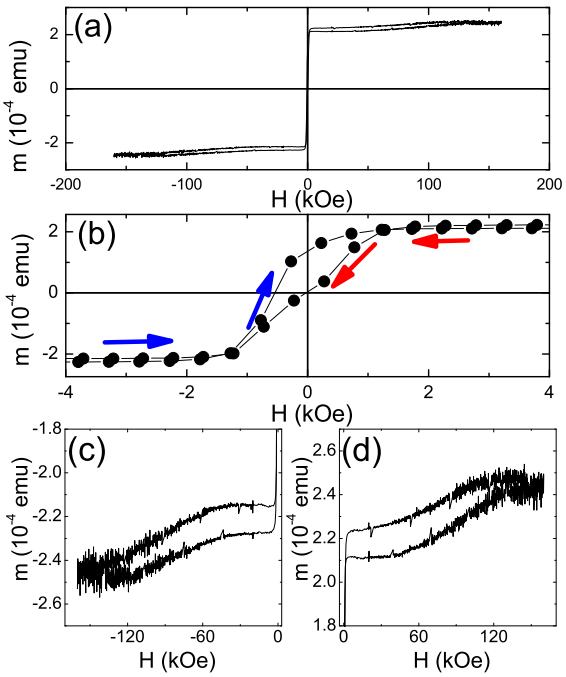

FIG. 4. (Color Online) (a) Hysteresis loop of $Fe_{0.45}Ni_{0.55}F_2$/Co at $T = 30$ K measured between $H = \pm 160$ kOe after field cooling from room temperature in $H_{CF} = 2.0$ kOe. (b) Magnification of the same data for small fields. The red arrows indicate the data with decreasing field while the blue arrow indicate the data with increasing field. Magnification of data at large fields is shown in (c) and (d).

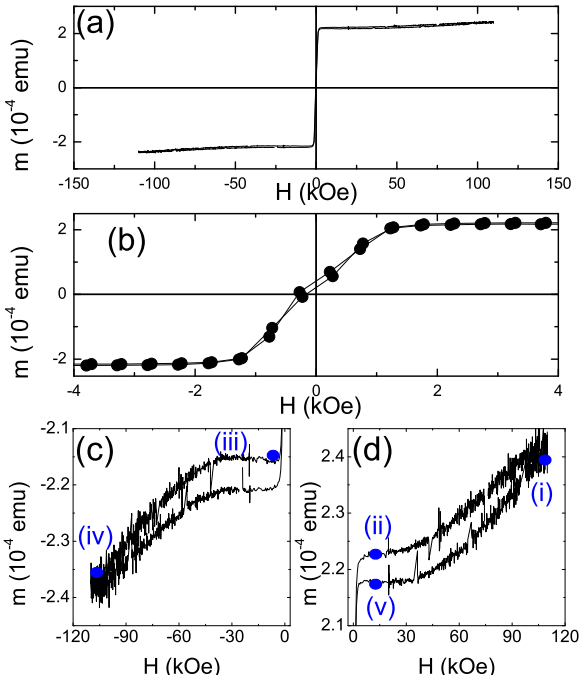

FIG. 5. (Color Online) (a) Hysteresis loop of the RAF/F $Fe_{0.45}Ni_{0.55}F_2$/Co sample at $T = 30$ K measured between $H = \pm 110$ kOe after field cooling at $H_{CF} = 2$ kOe. Magnification of the same data at small fields (b) and negative (c) and positive (d) fields are also shown.

TABLE II. Magnetization in emu/cm^3 at various fields for the interface and RAF layers of the $Fe_{0.45}Ni_{0.55}F_2$/Co sample determined from $\rho_m(z)$. The latin numerals refer to the fields in the hysteresis loop similarly labeled in Fig. 5.

Layer	(i) +110 kOe	(ii) +10 kOe	(iii) −10 kOe	(iv) −110 kOe	(v) +10 kOe
Interface	24 ± 11	7 ± 14	42 ± 11	-42 ± 11	-67 ± 11
$FeNiF_2$	32 ± 11	24 ± 11	28 ± 11	-56 ± 14	-28 ± 18

Magnetization measurements in the range of $H = \pm 110$ kOe, shown in Fig. 5, were also performed because it was the maximum field available for the PNR measurements. Compared to the $H = 160$ kOe measurements, the low field and high field hysteresis is smaller, as shown in Figs. 5(b)–(d), with a measured $\Delta M_S = (0.04 \pm 0.02) \times 10^{-4}$ emu. This indicates that the pinned magnetization was partially reversed. The data points labeled (i)-(v) in Figs. 5(c) and 5(d) are the fields at which PNR measurements were made. The PNR data and the corresponding fits are shown in Fig. 6 while Table II shows the magnetization values at the center of the interface and AF layers. The $M(z)$ profiles obtained from the fits are shown in Fig. 7. Recently, these magnetization profiles have been analyzed using the concepts of pinned and unpinned magnetizations in the antiferromagnetic, interface, and ferromagnetic layers.[13] It is important to note, however, that the terms "pinned" and "unpinned" normally refer to magnetic moments at low fields. At large enough fields, even the pinned magnetization can be reversed. Therefore, in the discussion referring to the RAF/F system which was measured in large fields, we do not refer to pinned and unpinned moments, but rather to the magnetization profile at each field.

Fig. 8 illustrates the magnetization component along the applied field axis at points (i)–(v) in Fig. 5 based on the PNR data. The behavior can be explained as follows: When the field was lowered from $H = +110$ kOe (i) to $H = +10$ kOe (ii), the interface magnetization decreased while the bulk RAF magnetization remained almost unchanged, indicating that the RAF/F antiferromagnetic exchange interaction was not quite strong enough to completely reverse the net magnetization in the RAF. Once the field was lowered further to $H = -10$ kOe (iii) and the F magnetization was reversed, the interface magnetization once again became large and aligned antiparallel to the F as a result of the interface antiferromagnetic interaction. When $H = -110$ kOe (iv), the field was strong enough to reverse the bulk RAF magnetization, causing the interface to align in the same direction. As the field was then increased to $H = +10$ kOe (v), a state similar (within the uncertainties of the magnetization values determined by PNR) to that

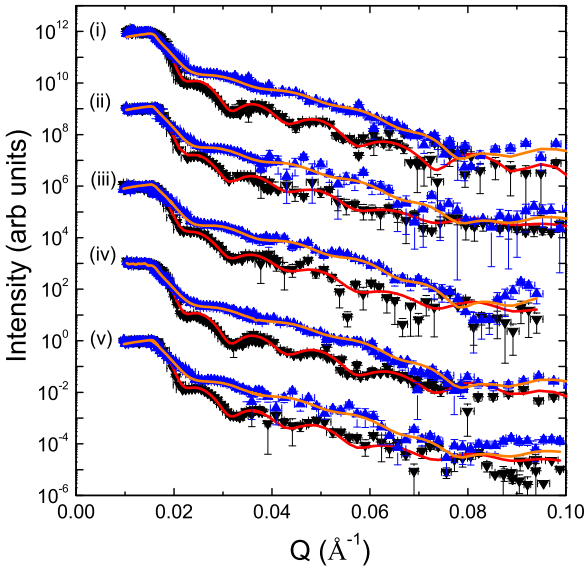

FIG. 6. (Color Online) PNR data measured at $T = 30$ K at fields corresponding to points (i)–(v) indicated in Fig. 5 for the DAF/F $Fe_{0.45}Ni_{0.55}F_2$/Co sample. The R^{--} data are the blue upright triangles and the R^{++} are the black inverted triangles. The solid orange and red lines are the fits to the R^{--} and R^{++} data respectively.

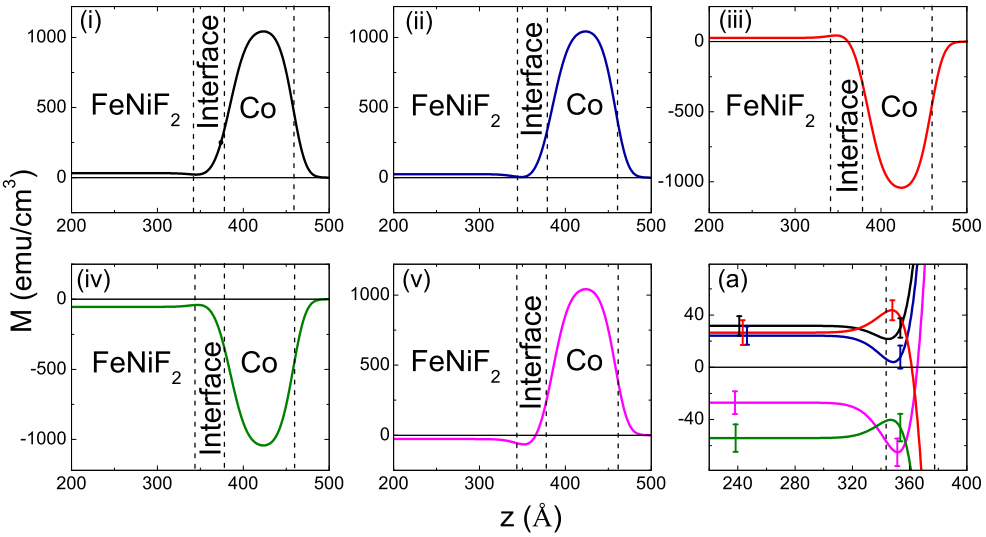

FIG. 7. (Color Online) (a) Depth profile of magnetization obtained from the PNR data at $T = 30$ K for the RAF/F $Fe_{0.45}Ni_{0.55}F_2$/Co sample. Panels (i)–(v) correspond to data obtained at the fields labeled (i)–(v) in Fig. 5. The vertical dotted lines indicate the position of the layer interfaces obtained from PNR. Panel (a) is a close-up of the data near the interface layer between the DAF and the F, with the line colors corresponding to the data in panels (i)–(v). Error bars indicate the uncertainty in the magnetization obtained from fits of PNR data. The region between vertical dotted lines denotes the position of the interface layer.

obtained at $H = -10$ kOe (iii) was achieved, with all magnetization components reversed as expected. The different magnetic configurations at the two $H = +10$ kOe fields [(ii) and (v)] explains the hysteretic behavior at high fields, which was due to a gradual reversal of the of the bulk RAF magnetization.

It is also interesting to compare the present results with the prior work of Fitzsimmons et al. where the pinned and unpinned magnetizations were studied via PNR in an AF/F FeF_2/Co bilayer.[13] The sample studied in Ref. 13 had both negative and positive EB, depending on the cooling field magnitude, and both states were studied, although measurement fields ($H = \pm 7$ kOe) were not large enough to reverse the pinned magnetization. For the positive EB

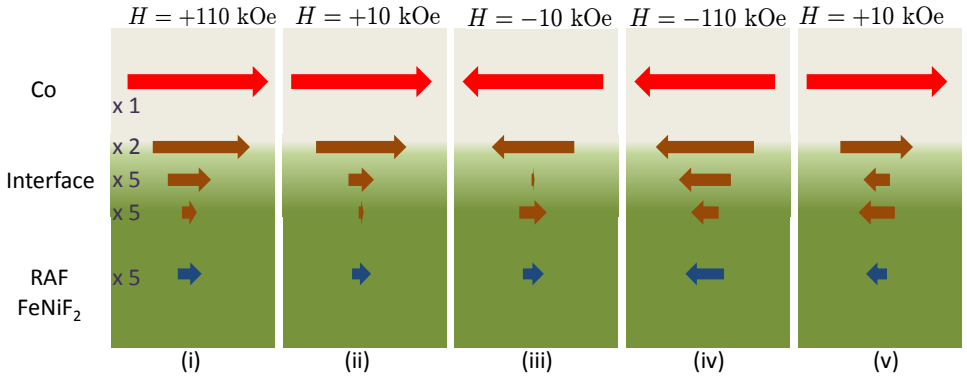

FIG. 8. (Color Online) Summary of magnetic configuration of the layers for the RAF/F $Fe_{0.45}Ni_{0.55}F_2$/Co sample obtained from the PNR data. The red arrow in the top layer is the magnetization at the center of the Co ferromagnetic layer. The three brown arrows in the middle represent the magnetization profile in the interface layer near the Co layer, the center, and the RAF layer. The dark blue arrow at the bottom is the magnetization in the bulk of the RAF. The arrows are drawn to scale but magnified as indicated on the left hand side of the diagram and provide a visual representation of the magnetization as deduced from Fig. 7.

state, we compare the RAF/F system at points (ii) and (iii) in the hysteresis curve (see Fig. 8) with the positive EB state in FeF_2/Co (bottom of Fig. 8 in Ref. 13). We find similar results for the case of the DAF, namely, a pinned magnetization in the DAF and magnetization reversal in the interface layer. Our data also indicate that a domain-wall state was formed at the interface by uncompensated magnetization at points (iii) and (v), as shown in Fig. 8, which are the two exchange-biased states probed by the experiment. This is consistent with the model proposed by Mauri et al. which explained EB in terms of an interface domain wall extending into the antiferromagnet created when the F layer's magnetization is reversed, similar to a spring magnet.[32] In our case, however, this domain wall is composed of uncompensated spins at the interface, and is ≈ 35 Å wide, according to the data in Table I. This result is thus consistent with the mechanism studied by Kiwi et al. where an incomplete domain wall in the ferromagnet is formed during magnetization reversal,[33] except that in our case this wall is confined to the interface itself. This also means that there is a minimum AF layer thickness for positive EB to occur which is on the order of the interface domain wall thickness.

B. DAF/F $Fe_{0.34}Zn_{0.66}F_2/FeF_2$/Co Sample

Figure 9(a) shows the XRR data and the corresponding fit while Fig. 9(b) shows $\rho_{xr}(z)$ and $d\rho_{xr}/dz$ obtained from the fits. The best fitting parameters for t, σ, and M, and their associated uncertainties are listed in Table III.

Figure 10 shows the magnetic moment of the $Fe_{0.34}Zn_{0.66}F_2$/Co DAF/F sample with $H_E = -260$ Oe and $\Delta M_S/M_S = +0.03 \pm 0.01$. The negative H_E and positive ΔM_S disappeared at $T = 25$ K. The hysteresis loops at $T = 5$ K were independent of the cooling field in the $H_{CF} = 100$ Oe to -7500 Oe range. PNR measurements were performed at $H = \pm 6.5$ kOe as indicated by the arrows in Fig. 10. The data with the best fit to the model are shown in Fig. 11. The Fe and Zn concentrations determined from x-ray diffaction measurements of the [001] lattice parameter[9] agreed well with ρ_n values obtained from the XRR and PNR fits as shown in Table III. Note that an additional interface layer was introduced between the DAF and the AF FeF_2 layer. For the PNR scattering length density profile, we refer to the interface layer as a combination of the interface and FeF_2 layers since the small thickness of each does not warrant a differentiation between them.

Figure 12(a) shows the depth profile of the magnetization from fitting the PNR profiles at $H = +6.5$ kOe (magenta curve) and $H = -6.5$ kOe (green curve), with the vertical dotted lines indicating the positions of the interfaces. In this case, we use the concepts of pinned and unpinned components, $M_P(z)$ and $M_U(z)$, respectively, defined by $M(\pm H) = M_P \pm |M_U|$ with $M_U(-H) = -M_U$. Solving for M_U and M_P yields $M_U = [M(+H) - M(-H)]/2$ and $M_P = [M(+H) + M(-H)]/2$.[13] For the DAF/F sample we compare the magnetization profile at $H = -6.5$ kOe with the one at $H = +6.5$ kOe. The resulting $M_P(z)$ and $M_U(z)$ profiles are shown in Fig. 12(b) by the blue and red curves, respectively. The profiles show the presence of an uncompensated magnetization parallel to the cooling field and the Co magnetization, which indicates the existence of ferromagnetic coupling between the Co and the $Fe_{0.34}Zn_{0.66}F_2/FeF_2$ layer. By integrating the depth profile of $M_P(z)$, the total pinned magnetic moment was calculated to be $\Delta M_S/M_S = 0.05 \pm 0.01$. This is comparable to the result of $\Delta M_S/M_S = 0.03 \pm 0.01$ obtained from

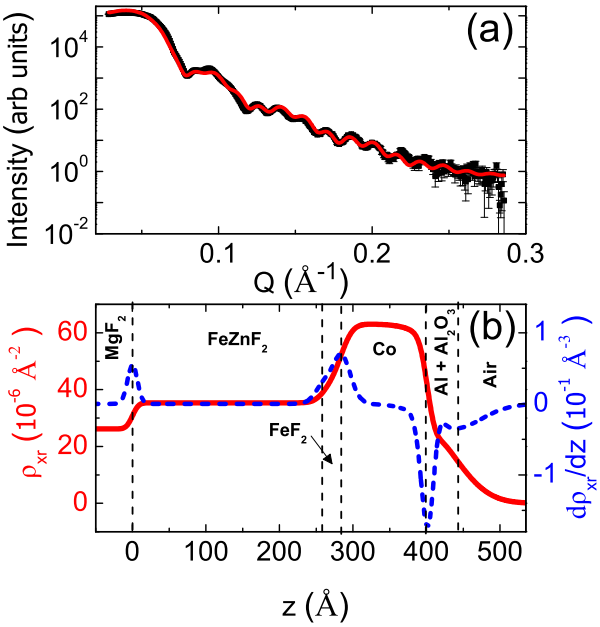

FIG. 9. (Color Online) (a) X-ray reflectivity measurements (black dots) and fit (red curve) of the DAF/F $Fe_{0.34}Zn_{0.66}F_2/FeF_2/Co$ sample. (b) Nuclear scattering length density profile (red curve) and the derivative of the scattering length density profile (blue dashed curve) obtained from the x-ray reflectivity fit.

TABLE III. Structural and magnetic fitting parameters for PNR and XRR data for the DAF/F $Fe_{0.34}Zn_{0.66}F_2/FeF_2/Co$ sample. Interface roughness σ and layer thickness t parameters are in Å the nuclear and x-ray charge scattering length densities, ρ_n and ρ_{xr}, are in 10^{-6} Å^{-2}, and the magnetizations M, determined from $\rho_m(z)$, are in emu/cm^3. The fields at which PNR measurements were performed are indicated. Parameters without uncertainties were kept constant during the fitting procedure.

Layer	Parameter	PNR		XRR
		+6.5 kOe	−6.5 kOe	
Al_2O_3	ρ_n, ρ_{xr}	0.97	0.97 ± 0.07	10.1
	σ	10	10 ± 5	14 ± 5
	t	34	22 ± 7	21 ± 4
Al	ρ_n, ρ_{xr}	1.79	1.79 ± 0.05	16.6
	σ	12	12 ± 5	15 ± 6
	t	23	23 ± 6	23 ± 5
Co	ρ_n, ρ_{xr}	2.16	2.16	62.9
	M	1195 ± 18	-1198 ± 18	
	σ	11	11 ± 6	12 ± 4
	t	126	126 ± 9	114 ± 5
Interface/FeF_2	ρ_n, ρ_{xr}	3.34	3.34 ± 0.04	46 ± 1
	M	634 ± 11	-648 ± 11	
	σ	6	6 ± 5	5 ± 2
	t	21	21 ± 6	26 ± 3
$Fe_{0.34}Zn_{0.66}F_2$	ρ_n, ρ_{xr}	5.22	5.22 ± 0.05	35 ± 1
	M	-21 ± 11	60 ± 11	
	σ	14	14 ± 6	10 ± 2
	t	254	254 ± 8	259 ± 4
MgF_2	ρ_n, ρ_{xr}	5.1	5.1	26.2
(Substrate)	σ	6	6 ± 3	3.9 ± 0.7

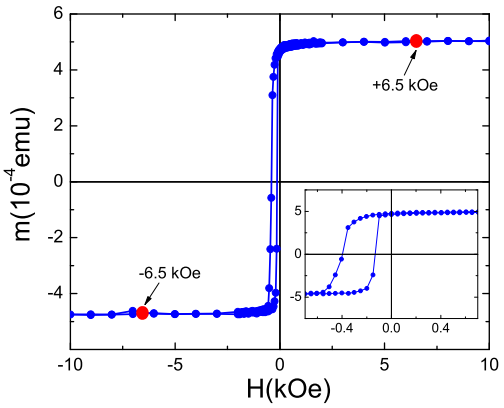

FIG. 10. (Color Online) Hysteresis loop at $T = 5$ K after cooling down from $T = 95$ K with $H_{CF} = 2.0$ kOe along the [001] direction. Polarized neutron reflectivity measurements were performed at $H = \pm 6.5$ kOe, indicated by the red circles. Inset: Close-up of hysteresis loop for small magnetic fields showing the negative EB.

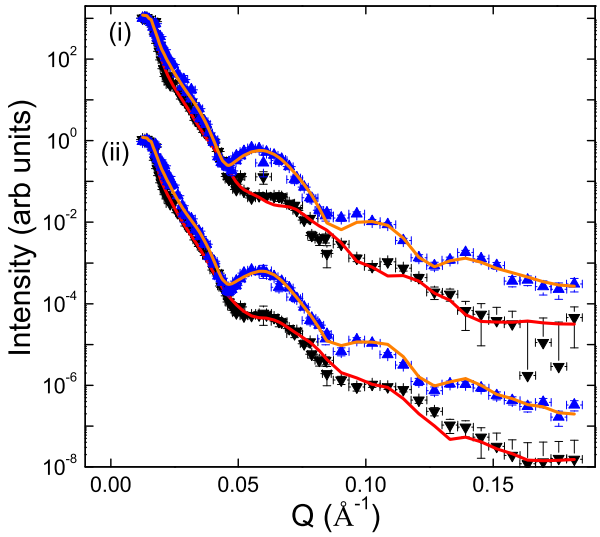

FIG. 11. (Color Online) PNR Profiles measured at $T = 5$ K for (i) $H = +6.5$ kOe and (ii) $H = -6.5$ kOe for the DAF/F $Fe_{0.34}Zn_{0.66}F_2$/Co sample. The R^{++} data are the blue upright triangles and the R^{--} are the black inverted triangles. The solid orange and red curves are the fits to the R^{++} and R^{--} data, respectively.

the direct magnetization measurements. The pinned magnetization at the interface was very small and the sign of the magnetization was not clear, as indicated in the inset of Fig. 12(b).

For FeF_2/Co bilayers in the negative EB state, Fitzsimmons et al. found both M_P and $M_U \neq 0$ at the interface, with most of the *net* interface magnetization being zero at $H = -7$ kOe, and $M_P = 0$ in the AF.[13] Our DAF/F sample with negative exchange bias, on the other hand, had a large $M_U \approx 640$ emu/cm^3 and $M_P \approx 0$ at the interface, and significant amounts of $M_P \approx 20$ emu/cm^3 and $M_U \approx -45$ emu/cm^3 in the DAF, as shown in Fig. 12. This means that in the field-cooled state the DAF forms domains, as proposed by the domain state model. In the domain state model, a DAF forms domains each with a net magnetization due to uncompensated spins at the domain boundaries.[5,7] Our results indicate that these domains are magnetically disordered in the field-cooled state. If this were not the case, a positive magnetization would have been measured in the DAF with PNR at $H = +6.5$ kOe, but instead the bulk DAF magnetization was zero [see Fig. 12(a)]. This is illustrated in Fig. 13, which shows the pinned (white arrows) and unpinned (red arrows) magnetization components at the two measurement fields. This means that some DAF magnetic grains were effectively antiferromagnetically coupled to the F layer, and reversed their magnetization with the F layer. Pinned domains also existed in the DAF, possibly due to a net ferromagnetic

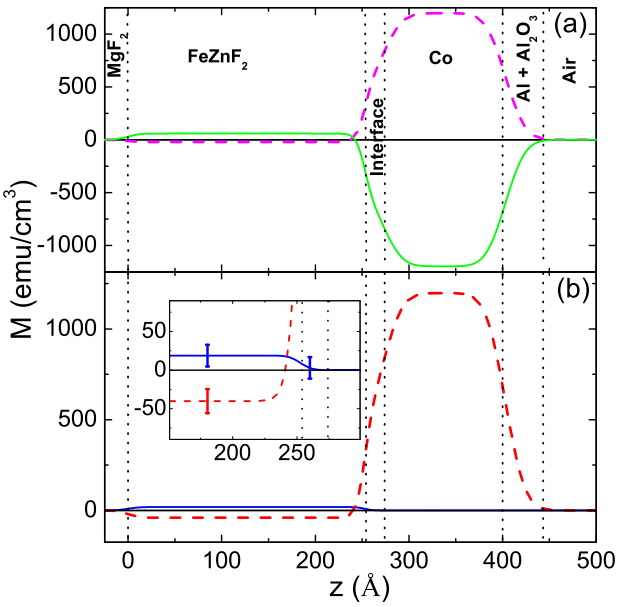

FIG. 12. (Color Online) (a) Depth profile of the magnetization from the PNR data at $T = 5$ K. The magenta dashed curve and solid green curve correspond to $H = +6.5$ kOe and $H = -6.5$ kOe, respectively. (b) Depth profile of the pinned and unpinned magnetizations (solid blue and dashed red curves, respectively) calculated for $H = -6.5$ kOe with respect to $H = +6.5$ kOe. The vertical dotted lines indicate the position of the interfaces, with the substrate-film interface set to $z = 0$.

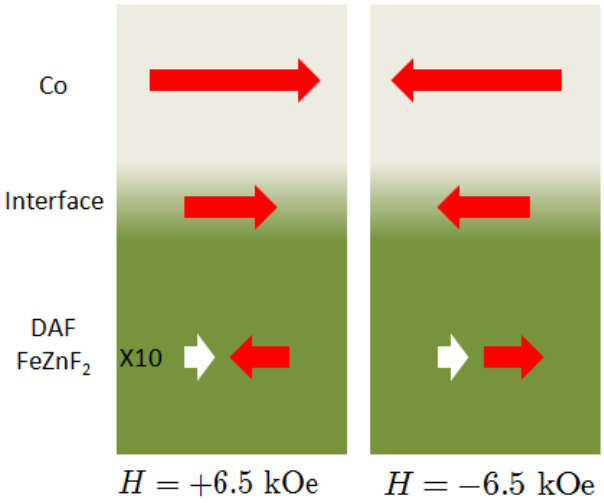

FIG. 13. (Color Online) Summary of pinned and unpinned magnetizations in each layer for the DAF/F $Fe_{0.45}Ni_{0.55}F_2$/Co sample obtained from the PNR data. Red arrows indicate unpinned magnetization components and white arrows in DAF layer signify pinned magnetization components. The arrows are drawn to scale as indicated.

interaction with the F layer. An antiferromagnetic interaction slightly stronger than the ferromagnetic interaction would cause the antiferromagnetically coupled domains to reverse, explaining $M_U < 0$, with the ferromagnetically coupled DAF domains being stabilized by dipole-dipole interactions with other DAF domains. Therefore, the exchange bias mechanism in the DAF/F system is significantly different from the AF/F system, and also from the RAF/F system discussed above. Also, the domain state model appears to be a simplification of the actual situation, since it does not take into account differing interfacial interactions and effective magnetic interactions between DAF grains. Finally, we note that this mechanism is similar to the one proposed by Malozemoff, where disorder at the interface can cause local random interface exchange contributions which can result in a net exchange bias by cooling the system into a disordered AF state.[34–36] In our case, the disorder is exacerbated by the randomly placed non-magnetic impurities which make it easy to form an AF domain structure.

IV. CONCLUSIONS

The depth profiles of the pinned and unpinned magnetization obtained by fitting the PNR data showed that at the interface there was a pinned component of magnetization that resulted in antiferromagnetic coupling in the RAF/F $Fe_{0.45}Ni_{0.55}F_2$/Co sample and in ferromagnetic coupling in the DAF/F $Fe_{0.34}Zn_{0.66}F_2/FeF_2$/Co sample. Moreover, a pinned magnetization was measured in both samples in the bulk of the DAF and RAF layers. By applying large fields in the RAF/F sample it was possible to study the reversal of both the interface and bulk RAF pinned magnetization. It was found that the interface magnetization is antiferromagnetically coupled to the ferromagnet, but either the RAF anisotropy in this particular sample was not weak enough or the RAF pinned magnetization was too large to permit complete reversal due to the interface coupling. This explains the large fields required to reverse the RAF magnetization and the reversed hysteresis loop observed in low field region. We have also identified the existence of a domain wall at the RAF/F interface which results from an effective positive exchange bias. For the DAF/F system, we have found evidence for the formation of a complex magnetic structure in the DAF, with domains antiferromagnetically coupled to the ferromagnet being reversed, while domains ferromagnetically coupled to the ferromagnet remaining pinned. This behavior is significantly different from that observed for the RAF system, as well as for previous work in AF/F bilayers, and can be explained by a different coupling strength of the two types of domains to the ferromagnet combined with a magnetic interaction (dipole-dipole) between the domains.

ACKNOWLEDGMENTS

The support of the National Science Foundation (grants No. DMR-0400578 and DMR-0903861) at WVU is gratefully acknowledged. At Los Alamos, this work was supported by the Office of Basic Energy Science, U. S. Department of Energy, BES-DMS funded by the Department of Energy's Office of Basic Energy Science. Los Alamos National Laboratory is operated by Los Alamos National Security LLC under DOE Contract DE-AC52-06NA25396.

* kmunbodh@mix.wvu.edu

[1] W. H. Meiklejohn and C. P. Bean, Phys. Rev. **102**, 1413 (1956).
[2] J. Nogués and I. K. Schuller, J. Magn. Magn. Mater. **192**, 203 (1999).
[3] A. E. Berkowitz and K. Takano, J. Magn. Magn. Mater. **200**, 552 (1999).
[4] M. Kiwi, J. Magn. Magn. Mater. **234**, 584 (2001).
[5] P. Miltényi, M. Gierlings, J. Keller, B. Beschoten, G. Güntherodt, U. Nowak, and K. D. Usadel, Phys. Rev. Lett. **84**, 4224 (2000).
[6] J.-I. Hong, T. Leo, D. J. Smith, and A. E. Berkowitz, Phys. Rev. Lett. **96**, 117204 (2006).
[7] U. Nowak, K. D. Usadel, J. Keller, P. Miltényi, B. Beschoten, and G. Guntherodt, Phys. Rev. B **66**, 014430 (2002).
[8] D. Belanger and A. Young, J. Magn. Magn. Mater. **100**, 272 (1991).
[9] H. Shi, D. Lederman, and E. E. Fullerton, J. Appl. Phys. **91**, 7763 (2002).
[10] H. Shi, Z. Liu, and D. Lederman, Phys. Rev. B **72**, 224417 (2005).
[11] S. Roy, M. R. Fitzsimmons, S. Park, M. Dorn, O. Petracic, I. V. Roshchin, Z.-P. Li, X. Batlle, R. Morales, A. Misra, X. Zhang, K. Chesnel, J. B. Kortright, S. K. Sinha, and I. K. Schuller, Phys. Rev. Lett. **95**, 047201 (2005).
[12] H. Ohldag, H. Shi, E. Arenholz, J. Stöhr, and D. Lederman, Phys. Rev. Lett. **96**, 027203 (2006).
[13] M. R. Fitzsimmons, B. J. Kirby, S. Roy, Z.-P. Li, I. V. Roshchin, S. K. Sinha, and I. K. Schuller, Phys. Rev. B **75**, 214412 (2007).
[14] J. Nogués, C. Leighton, and I. K. Schuller, Phys. Rev. B **61**, 1315 (2000).
[15] M. Cheon, Z. Liu, and D. Lederman, J. Appl. Phys. **101**, 09E503 (2007).
[16] J. W. Stout and S. A. Reed, J. Am. Chem. Soc. **76**, 5279 (1954).
[17] M. T. Hutchings, B. D. Rainford, and H. J. Guggenheim, J. Phys. C: Solid State Phys. **3**, 307 (1970).
[18] D. P. Belanger and H. Yoshizawa, Phys. Rev. B **35**, 4823 (1987).
[19] M. T. Hutchings, M. F. Thorpe, R. J. Birgeneau, P. A. Fleury, and H. J. Guggenheim, Phys. Rev. B **2**, 1362 (1970).
[20] H. Shi, D. Lederman, K. V. O'Donovan, and J. A. Borchers, Phys. Rev. B **69**, 214416 (2004).
[21] T. Moriya, Phys. Rev. **117**, 635 (1960).
[22] J. Nogués, D. Lederman, T. J. Moran, I. K. Schuller, and K. V. Rao, Appl. Phys. Lett. **68**, 3186 (1996).
[23] J. Nogués, D. Lederman, T. J. Moran, and I. K. Schuller, Phys. Rev. Lett. **76**, 4624 (1996).
[24] D. Lederman, J. Nogués, and I. K. Schuller, Phys. Rev. B **56**, 2332 (1997).
[25] C. Leighton, J. Nogués, H. Suhl, and I. K. Schuller, Phys. Rev. B **60**, 12837 (1999).
[26] M. Cheon, Z. Liu, and D. Lederman, Appl. Phys. Lett. **90**, 012511 (2007).
[27] M. Björck and G. Andersson, J. Appl. Cryst. **40**, 1174 (2007).
[28] L. G. Parratt, Phys. Rev. **95**, 359 (1954).
[29] K. Munbodh, F. A. Perez, C. Keenan, D. Lederman, M. Zhernenkov, and M. R. Fitzsimmons, Phys. Rev. B **83**, 094432 (2011).
[30] G. Mastrogiacomo, J. F. Löffler, and N. R. Dilley, Appl. Phys. Lett. **92**, 082501 (2008).
[31] S. Park, M. R. Fitzsimmons, C. F. Majkrzak, B. D. Schultz, and C. J. Palmström, J. Appl. Phys. **104**, 083905 (2008).
[32] D. Mauri, H. C. Siegmann, P. S. Bagus, and E. Kay, J. Appl. Phys. **62**, 3047 (1987).
[33] M. Kiwi, J. Mejía-López, R. D. Portugal, and R. Ramírez, Europhys. Lett. **48**, 573 (1999).
[34] A. P. Malozemoff, Phys. Rev. B **35**, 3679 (1987).
[35] A. P. Malozemoff, J. Appl. Phys. **63**, 3874 (1988).
[36] A. P. Malozemoff, Phys. Rev. B **37**, 7673 (1988).